

## Influence of Clip Locations on Intraaneurysmal Flow Dynamics in Patient-specific Anterior Communicating Aneurysm Models with Different Aneurysmal Angle

Lizhong Mu<sup>1,\*</sup>, Qingzhuo Chi<sup>1</sup>, Changjin Ji<sup>2</sup>, Ying He<sup>1</sup> and Ge Gao<sup>3</sup>

**Abstract:** To improve aneurysm treatment, this study examined the influence of clip locations on hemodynamic factors in patient-specific anterior communicating artery (ACoA) aneurysms with different aneurysmal angle. We proposed a simplified classification of ACoA aneurysms using aneurysmal angle, defined by the angle of pivot of the aneurysmal dome and the virtual two-dimensional plane created by both proximal A2 segments of anterior cerebral artery (ACA). ACoA aneurysms with three different aneurysmal angles, which are 15°, 80° and 120°, were analyzed in our study. In this work, we obtained hemodynamics before and after clipping surgery with three clip locations based on clinical clipping strategies in three ACoA aneurysms with different aneurysm angles. Results showed that local high pressure occurs at impingement region of the ACoA aneurysm before clipping and new impingement region close to the clipping location after clipping treatment. For clipping the aneurysm with aneurysmal angle 15° and a wide neck, wall shear stress (WSS) distribution is more uniform when the clipping angle of two clips close to 180° comparing with other two angles. In addition, for clipping the aneurysm with aneurysmal angle 80° and 120°, local high pressure appears on new impingement region and high WSS distributes around the clipping location when the clip plane is normal to the direction of inflow of aneurysm from the dominance of A1 segment of ACA. Hence, we should avoid the impingement of inflow from the A1 segment and choose a favorable clipping location for the fastness of clip. The results of our study could preoperatively give a useful information to the decision of surgical plan.

**Keywords:** Intracranial aneurysm, anterior communicating artery, surgical clipping treatment, patient-specific model, intraaneurysmal flow dynamics.

### 1 Introduction

The anterior communicating artery (ACoA) is one of frequent sites of intracranial aneurysms occurrences, which are pathological dilatations of the vessel wall and generally occur near arterial bifurcations in the circle of Willis (CoW) [Lasheras (2007);

<sup>1</sup> Key laboratory of Ocean Energy Utilization and Energy Conservation of Ministry of Education, School of Energy and Power Engineering, Dalian University of Technology, No. 2 Linggong Road, Dalian, 116024, China.

<sup>2</sup> School of Biomedical Engineering, Capital Medical University, Beijing, 100069, China.

<sup>3</sup> The First Affiliated Hospital of University of Science and Technology of China, Hefei, 230036, China.

\* Corresponding Author: Lizhong Mu. Email: muliz@dlut.edu.cn.

Liu, Cai, Chen et al. (2017)]. The anterior communicating artery is an important artery in the CoW and serves as a bridge connecting the left and right anterior cerebral arteries (ACA) [Cieslicki and Ciesla (2005)]. The flow rate and wall shear stress (WSS) in the ACoA are low when the CoW is completely functional, but may increase as unilateral stenosis or agenesis occur in the A1 segments of the ACA [Jou, Lee and Mawad (2010)]. The increased WSS in the ACoA is a potential risk factor for the formation of ACoA aneurysm [Alastruey, Parker, Peiró et al. (2007)].

Currently, endovascular techniques and surgical clipping are the most common methods of intracranial aneurysm treatment [Molyneux, Kerr, Stratton et al. (2002)]. To occlude blood flow into the aneurysm sac, balloons or microcoils access the aneurysm via arteries, and embolization of the aneurysm is accomplished with thrombus formation during endovascular treatment. To treat an aneurysm with a wide neck, balloon-expandable coronary stents are usually placed to support coil embolization, and a titanium clip is located at the neck of the aneurysm to occlude blood flow.

In clinic, the clipping strategy of ACoA aneurysm has been reported to be deeply related to its classification [Nossek, Setton, Karimi et al. (2016); Wang, Xu and Xu (2017)]. There are several proposed classification systems for ACoA aneurysms, which are based on the positional relation of aneurysmal dome to the ACoA. 6 directions, anterior, superior, posterior, inferior, medial and lateral, were used by Matsukawa et al. [Matsukawa, Uemura, Fujii et al. (2013)] to classify the direction of ACoA aneurysmal dome. In the work of Hernesniemi et al. [Hernesniemi, Dashti, Lehecka et al. (2008a)], the ACoA aneurysms were classified into four groups, downward, forward, upward and backward according to the direction of the dome. Three types of superiorly projecting ACoA aneurysms were summarized by Nossek et al. [Nossek, Setton, Karimi et al. (2016)] based on the relationship of the aneurysm to the virtual plane where the A2 segments located. Type 1 was defined when the aneurysmal dome is bisected by the virtual plane created by both proximal A2 segments. The clip is set parallel to the communicating artery in this type. When the aneurysm neck is much wider than the diameter of the mother vessels, two or more clips are used together to completely clip the aneurysm. Type 2 was defined as the case that the aneurysm dome projection is posterior to this virtual plane. A straight clip is usually set parallel to ACoA during treatment and does not locate in the virtual two-dimensional plane. Type 3 was defined by sagittal rotation of the plane. The direction of clip will be set normal to the communicating artery. However, it is not always possible to realize a complete occlusion of aneurysm neck due to complex spatial structure. There is a risk of aneurysm recurrence from slippage of the aneurysm clip or compaction of the coil, and even enlargement of the residual portion of the aneurysm neck [Wu, Yang, Huang et al. (2013b)]. The risk of aneurysm recurrence after treatment is related not only to the characteristics of the aneurysm but also to the hemodynamics in the residual portion of aneurysm neck.

Hemodynamic changes such as displacement distribution and WSS in the residual portion of the aneurysm neck are believed to correlate with aneurysm recurrence after treatment. Numerical analysis and *in vitro* experiments offer a good way to understand the changes in hemodynamic factors. An idealized model has been widely used to investigate blood flow behavior after aneurysm treatment, in which the parent vessels are represented as

straight or curved tubes, and a spherical wall is used to simulate coil embolization. Byun et al. [Byun and Rhee (2004)] modeled four coil locations: The proximal/distal neck and proximal/distal dome of the aneurysm and found that the inflow rate is smallest in the distal neck occlusion model. Based on this work, Ahmed et al. [Ahmed, Šutalo and Kavnoudias (2006)] considered the pulsatile flow and non-linear deformation of the artery wall and reported that the maximum wall displacement occurred at the dome. From the above studies, we know that the flow field affects the coil location during endovascular treatment techniques. Gobin et al. [Gobin, Counord, Flaud et al. (1994)] investigated the influence of steady flow and pulsatile perfusion on flow pattern and pressure in an idealised *in vitro* model of a giant aneurysm, and found that the flow pattern within the aneurysm is affected mainly by the pulsatility and flow rate. Chodzyński et al. [Chodzyński, Eker, Vanrossomme et al. (2016)] took into account the influence of the gravity orientation of saccular aneurysms on the hemodynamics with and without a flow diverter stent, and found that the orientation of gravity influences the behavior of blood cells in the aneurysm after stenting.

In addition, the analysis based on patient-specific models, reconstructed from sequential images before and after aneurysm treatment, can directly indicate the changes in flow behavior in a cerebral aneurysm. Chen et al. [Chen, Wang, Ding et al. (2009)] compared blood flow behavior in a patient-specific model of the basilar artery before and after endovascular treatment, and found great differences in WSS and displacement distribution at the neck of the aneurysm. High WSS occurs near the neck of the aneurysm after treatment, which could be a potential risk factor for aneurysm recurrence. A vortex flow was found in the remnant neck of post-occlusion aneurysms [Irie, Anzai, Kojima et al. (2012); Ortega, Hartman, Rodriguez et al. (2008)]. The occurrence of concentrated swirling flow may increase WSS in the surrounding residual portion of the aneurysm neck, which would enlarge over time under sustained interaction with the vortex flow. Luo et al. [Luo, Yang, Wang et al. (2011)] found that high WSS appears near the neck in all five recanalized aneurysms, and the high WSS region is well-correlated with the location of recanalization. However, there are few studies on how clip location affects flow characteristics during surgical clipping treatment based on patient-specific model.

To improve clip treatment of aneurysm, it is necessary to understand how clip location in different types of ACoA aneurysms influences the change in hemodynamic factors. Hence, the purpose of this study was to investigate the effect of clipping location on intraaneurysmal flow dynamics in three patient-specific anterior communicating aneurysm models with different aneurysmal angle. To simplify the classification of ACoA aneurysms, an aneurysmal angle was defined by the angle of pivot of the aneurysmal dome and two-dimensional virtual plane created by both proximal A2 segments.

## 2 Materials and methods

### 2.1 Image acquisition

All the original CT images of ACoA aneurysms were obtained from the neurological surgery in the First Affiliated Hospital of the University of Science and Technology of China. Data of 12 patients with aneurysms were selected in the first half year of 2018,

who were suffering from subarachnoid hemorrhage (SAH) with ACoA aneurysms ruptured. Fig. 1 shows three cross-sectional images acquired in the circle of Willis in the region of an ACoA aneurysm and its reconstructed 3D model. The inter-slice distance and the in-plane resolution of the sequential CT images are 0.5 mm and 0.84 mm, respectively. The region of the ACoA aneurysm and the A2 segments of the ACA are clearly visible. Segmentation of all images and the reconstruction of 3D geometry were accomplished using the image processing package ScanIP (SIMPLEWARE Ltd., Exeter, UK). The interested region was segmented based on grayscale intensity of images firstly, a region growing method and morphological filters were used then to obtain the region of the circle of Willis and the aneurysm with smooth edge from each slice. Smoothing was performed via a recursive Gaussian filter based on a linear smoothing enhancement algorithm. 3D reconstruction was achieved by surface rendering, which outlined the contours of the anatomical structures from the masks of 2D images. In this study, the 3D ACoA model consisted mainly of the A1 and A2 segments of the ACA, and all 12 reconstructed ACoA aneurysm models are shown in Fig. 2a.

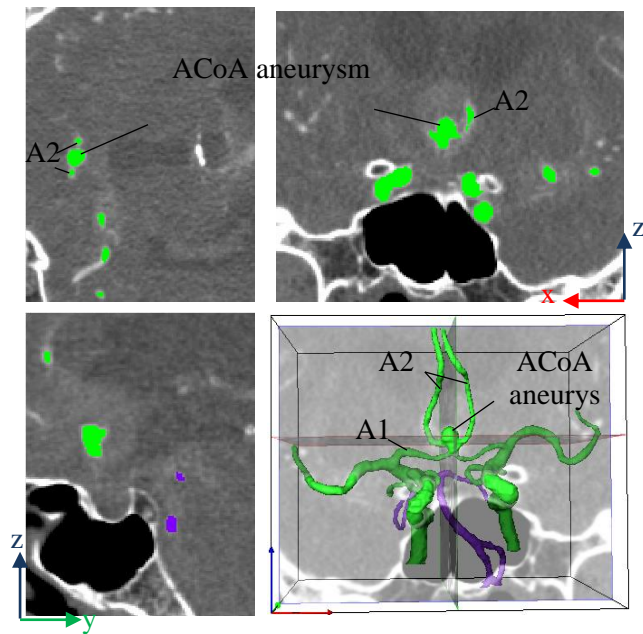


**Figure 1:** Circle of Willis with an ACoA aneurysm reconstruction (I-1 of Group I) in SIMPLEWARE

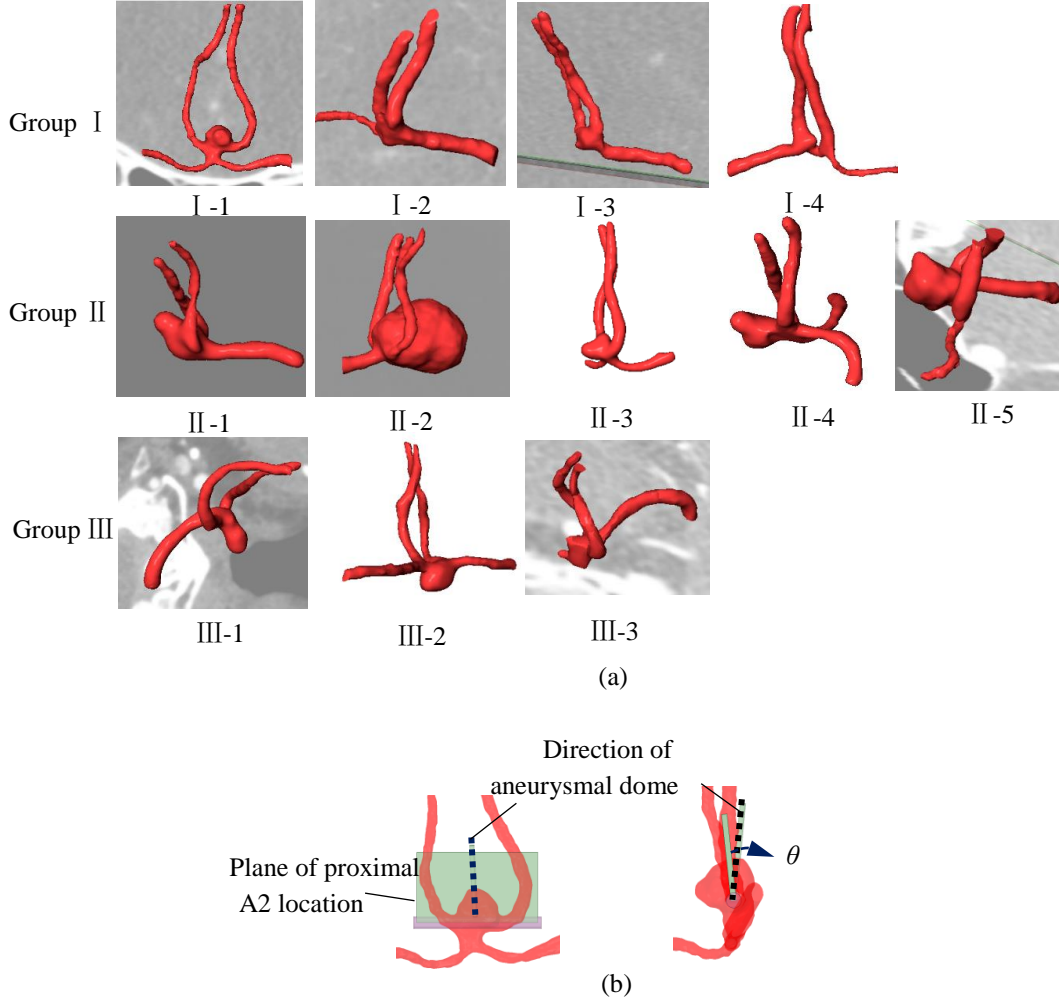


**Figure 2:** (a) ACoA aneurysm models classified by different aneurysmal angles  $\theta$ . Group I:  $30^\circ > \theta > 0^\circ$ ; Group II:  $90^\circ \geq \theta \geq 30^\circ$ , Group III:  $\theta > 90^\circ$ . (b) Definition of aneurysmal angle  $\theta$ , consisting of the aneurysmal direction and the plane of A2 segments location. Left one and right one are the front view and side view of an ACoA aneurysm

## 2.2 Quantification of aneurysm geometry and case selection

Several geometric parameters were included to assess the morphological features of an aneurysm, such as an aspect ratio [Lai, Tang, Tsang et al. (2016); Ujiie, Tachibana, Hiramatsu et al. (1999); Ujiie, Tamano, Sasaki et al. (2001)] and width of the aneurysmal neck [Campi, Ramzi, Molyneux et al. (2007); Teleb, Pandya, Castonguay et al. (2014)]. It was noticed that the relative locations of aneurysmal dome and A2 segments differed among the 12 specific-patient models in Fig. 2a. As previously mentioned, ACoA aneurysms were usually classified by considering the virtual plane created by the proximal A2 segments and its relationship to the aneurysmal dome, which is relevant to

the clipping location during microsurgery. Here, we defined a geometric parameter of aneurysmal angle, consisting of the direction of aneurysmal dome and 2D virtual plane created by the proximal A2 segments, as indicated in Fig. 2b. The determinations of the plane of the A2 segment location and aneurysmal direction and aneurysmal angle were accomplished using the Vascular Modeling Toolkit. A process of aneurysmal angle calculation is illustrated in Fig. 3. The direction of aneurysmal dome is defined by a vector of  $OE$ , and the plane of proximal A2 segments is determined by points  $D$ ,  $O$  and  $F$ . Angle  $EOG$  is then used to approximate its aneurysmal angle. Points  $B$  and  $C$  are the apices of the A2 segments;  $O$ , which is assumed to be located at ACoA, is the point with the maximum local distance from  $B$  and  $C$ ;  $D$  and  $F$  are the centres of the successive points which start from  $O$  with a number range of 15~20 points;  $E$  is the apex of the aneurysmal dome at the maximum distance from point  $O$ ; and  $G$  is the central point between  $D$  and  $F$ .

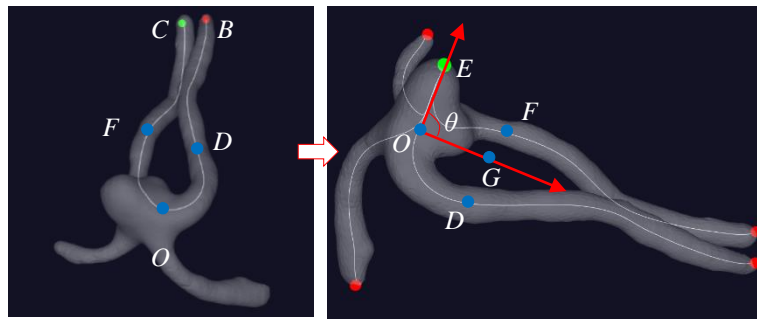


**Figure 3:** Determination of plane of A2 segments location, aneurysmal direction and aneurysmal angle in Vascular Modeling Toolkit. White lines indicate the centre lines of the vessels and aneurysm. The direction of aneurysmal dome is defined by a vector of  $OE$ , the plane of proximal A2 segments is determined by points  $D$ ,  $O$ , and  $F$ . Angle  $EOG$  approximates the aneurysmal angle. Where, points  $B$  and  $C$  are the apices of the A2 segments,  $O$  is the point with the local maximum distance from  $B$  and  $C$  and is assumed to be located at the ACoA,  $D$  and  $F$  are the centres of successive points from  $O$ , ranging in number from 15~20,  $E$  is the apex of the aneurysmal dome at the maximum distance from point  $O$ . And  $G$  is the centre point between  $D$  and  $F$

Fig. 4 shows the distribution of aneurysmal angles among 12 patient-specific models. We can see that the aneurysmal angles change due to the spatial structure of vascular branches. There are three types of circle of Willis structures in this study: Normal A1 segments of ACA, and unilateral hypoplasia or aplasia in the A1 segments of ACA. In this work, ACoA aneurysm structures can be classified into three groups by the aneurysm angle  $\theta$ , as indicated in Fig. 2a. Group I includes ACoA aneurysms with a small aneurysmal angle of 0° to 30°. For group II, the aneurysmal angle is in the range 30° to 90°, and in group III the aneurysmal angle is greater than 90°.

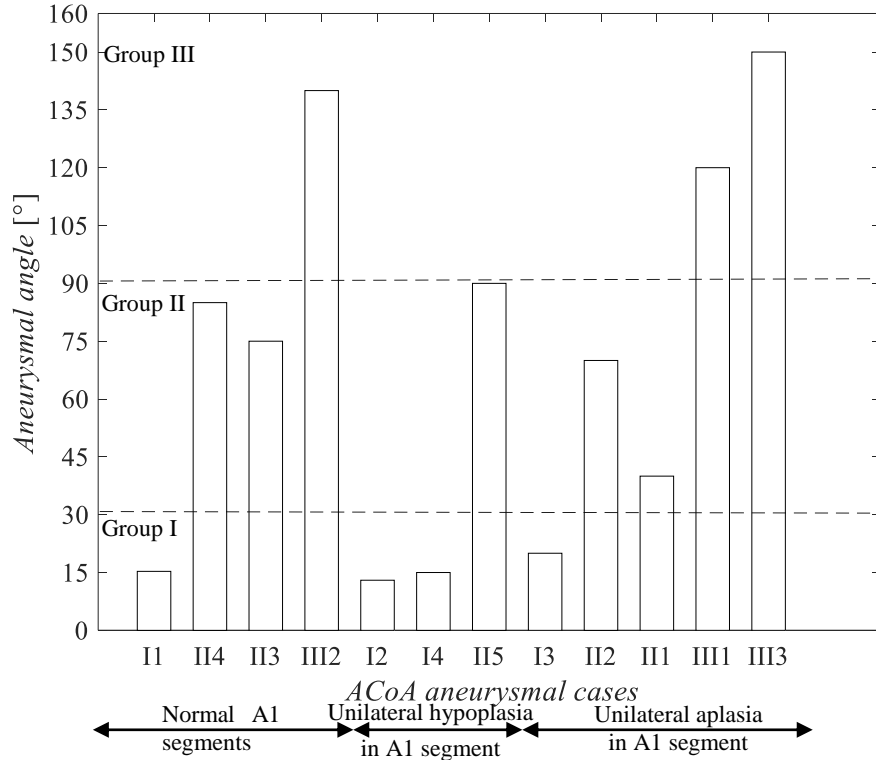


**Figure 4:** Aneurysmal angles distribution in 12 ACoA aneurysm cases

### 2.3 Model modification for surgical clipping simulation

In the work of Wang et al. [Wang, Xu and Xu (2017)], he compared the aneurysmal structures before and after surgical treatment by clipping, including a DSA detection and endoscope observation. It was found that the structure of the aneurysm is modified by the clip. A hill-shaped structure has clearly formed near the clip, which is a common characteristic of aneurysmal structure after surgical treatment. The 3D aneurysm model for simulating surgical clip treatment was generated by the following processes in SIMPLEWARE, as indicated in Fig. 5. First, the location and direction of clipping were fixed. The location of the hill top identified the clip position and the direction from hill bottom to its top defined the clipping direction, as indicated by the blue and red dotted arrows, respectively, in Fig. 5a. A virtual cube was applied to cut the aneurysm on both sides of the clipping direction (Figs. 5b and 5c). The topology of the aneurysmal neck after clipping was determined by the bottom of this cube. A smooth model was generated after using a recursive Gaussian filter.

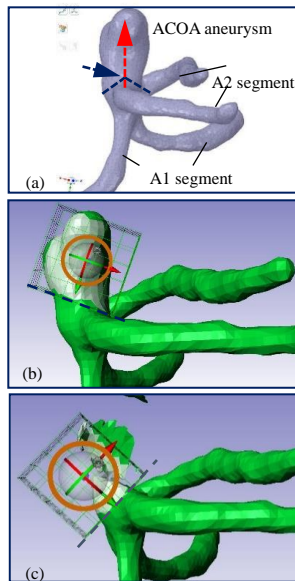


**Figure 5:** The virtual process for clipping ACoA aneurysm. (a) Dotted blue and red arrows indicate the locations and directions considered before clipping. (b-c) A virtual cube is applied to cut the original model from side to side. The topology of aneurysmal neck after clipping is determined by the bottom of this cube

A hollow elastic model of the ACoA aneurysm with and without clip was compared with the aneurysmal geometry (III-1) before and after virtual clipping process to verify this virtual surgical clipping method, as shown in Fig. 6. The hollow elastic model was manufactured with reference to a reported method [Amp and Dobos (2014); Arcaute and Wicker (2008); Mashiko, Otani, Kawano et al. (2015)]. A 3D computerized model of an aneurysm (Fig. 6a) with a resolution of 0.5 mm was input into a software used in 3D printer (GN-T2018, Shenyang Gaien), and a water-soluble print (PVA 3D filament, natural-0.5 kg (N.W.)) of the patient-specific aneurysm was obtained, and then surface polished and coated with double-component silicone (E620 AB Shenzhen Chunchang Group). A hollow elastic model of the ACoA aneurysm was generated after the water-soluble print melted in water at a temperature of 30°C for 20 min. As Fig. 6c shows, the hollow elastic model successfully reproduces the structure of the ACoA aneurysm. Comparing Figs. 6b and 6d, we can see that the 3D model of the ACoA aneurysm after surgical clipping agrees with its elastic structure with a clip at the neck. This virtual clipping method would be workable in simulating the surgical treatment of aneurysm.

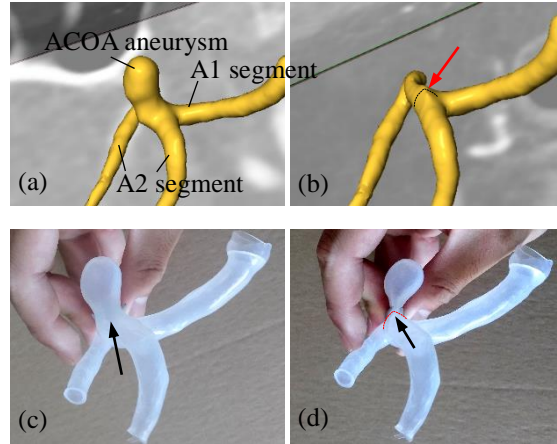


**Figure 6:** Comparison of an ACoA aneurysm structure before and after clip: (a, b) 3D reconstructed model, and (c, d) Hollow elastic model

#### 2.4 Computational mesh generation

A hybrid mesh consisting of tetrahedral grids inside and a prismatic boundary layer was generated using the ANSYS meshing system in ANSYS workbench. Two steps were developed to control the generation of the mesh. Because the calculation domain was obtained from an STL file, the first step was to insert the ‘Path Independent’ method that helps to control mesh generation and is useful for optimizing the distribution of the grid. An inflation layer with five layers and a growth rate of 1.1 was then generated all over the surface except for the inlets and outlets. After importing the calculation grids into Fluent 18.0, an additional grid processing operation was used to polyhedralise the mesh, which reduced the computation cost by about 50% by reducing the total elements from more than 12 million to 4 million. The appearance of mesh and the local mesh of ACoA aneurysm (III-1) at the inlet of the computational domain after polygonization are presented in Fig. 7a and Fig. 7b.

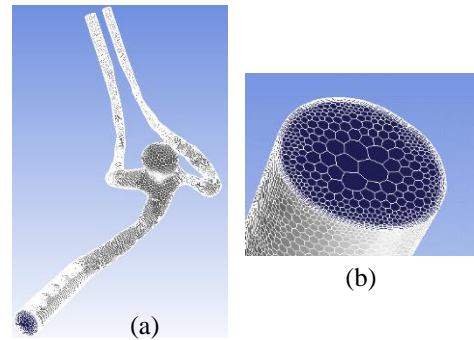


**Figure 7:** Overview of an ACoA aneurysm structure (III-1) with polygonal mesh (a) and its local meshes of inlet with boundary layers (b)

Several mesh-independent tests, which included volume average pressure, volume average velocity and average WSS, were carried out to improve the stability of the numerical simulation. Three meshing schemes were generated by increasing the node distribution and inflation layers for case 3: The coarse mesh contained 1,119,991 cells while the medium and fine mesh, under a refinement of 100%, contained 1,972,327 cells and 3,375,253 cells, respectively. In this numerical experiment, the truncation error was second-order. For the medium mesh, the relative changes in volume average pressure, volume average velocity and average WSS were about 0.36%, 0.54% and 0.26%, respectively. The relative changes for the fine mesh were about 0.14%, 0.31% and 0.26%, respectively. The medium mesh scheme was adopted because of its stable performance and reduced time cost.

### **2.5 Flow model and boundary conditions**

The blood used in the simulation was treated as a Newtonian and incompressible fluid [Chen, Wang, Ding et al. (2009); Cheng, Tan, Riga et al. (2010); Luo, Yang, Wang et al. (2011); Jhunjhunwala, Padole and Thombre (2016)] of a density  $\rho=1055 \text{ kg}\cdot\text{m}^{-3}$ , of a dynamic viscosity  $\nu=4.0 \text{ MPa}$ . The commercial CFD solver ANSYS FLUENT v.18.0 was used to approximately solve the Navier-Stokes equations with the assumption of a laminar, homogenous and incompressible blood flow. A rigid wall assumption was also used with a no-slip boundary condition, as wall motion is not believed to significantly alter high WSS regions [Olivieri, Zélicourt, Haggerty et al. (2011)]. The shear stress transport eddy-viscosity model was adopted to capture the WSS distribution [Kousera, Wood, Seed et al. (2013)]. As reported by Khan et al. [Khan, Valen-Sendstad, Steinman et al. (2015)], low-order schemes ironically need a higher mesh resolution. In this case, we set the spatial discretization as second-order upwind.

A boundary condition strategy was designed with an inflow inlet at the A1 segments and two pressure outlets at the A2 segments of the ACA. As reported by Mantha et al. [Mantha, Benndorf, Hernandez et al. (2009)], major aspects of the behavior of aneurysmal flow dynamics can be learned from steady, non-pulsatile inflow simulation, which is simpler and faster than time-dependent pulsatile flow. Researchers including Geers et al. [Geers, Larrabide, Morales et al. (2014)] and Karmonik et al. [Karmonik, Diaz, Klucznik et al. (2014)] have also confirmed that steady flow simulation can accurately approach the TA WSS field of a cerebral aneurysm. Hence, this study used a steady inflow boundary condition of 0.51 m/s inlet velocity at the A1 segments and 0 pressure outflow at the A2 segments of the ACA, based on the work of Xu et al. [Xu, Zhang, Wang et al. (2012)].

## **3 Results**

A CFD simulation was performed to investigate the influence on the flow characteristics of the clipping location in patient-specific ACoA aneurysms.

For comparing the flow dynamics of ACoA aneurysm with different aneurysm angles before and after vital clipping, three cases of ACoA structures were used in this study: model I-1 (case 1:  $\theta=15^\circ$ ), model II-4 (case 2:  $\theta=80^\circ$ ), model III-1 (case 3:  $\theta=120^\circ$ ) as shown in Fig. 2a. Firstly, hemodynamic factors, such as stream line, pressure and WSS,

were compared in ACoA aneurysms with aneurysm angle before and after clipping, as shown in Section 3.1. And then, we compared the pressure and WSS distribution in the aneurysms with different clipping location based on two clipping strategies shown in Section 3.2.

### ***3.1 Flow comparisons in ACoA aneurysms with different aneurysmal angle before and after clipping***

ACoA aneurysms with three aneurysm angles of  $\theta=15^\circ$ ,  $80^\circ$  and  $120^\circ$  were clipped in a similar way with the clipping plane normal to the direction of the aneurysm dome. A comparison of flow characteristics, i.e. streamline, pressure and WSS distribution are shown in Figs. 8-10. Complex flow impingement regions can be observed in all three cases before clipping treatment, with the blood flow entering the aneurysm sac through the impingement region and forming a large and complex vortex inside (Figs. 8a (i), 9a (i), 10a (i)). In addition, the impingement regions were found at the aneurysmal sidewall and close to the middle of aneurysmal neck. Local pressure is high in the impingement region, with high WSS at the neck of the aneurysm, as shown by the red arrow, and low WSS at the aneurysmal dome. This may be attributable to the coincidence of the direction of the aneurysmal sac with the direction of flow in the A1 segment feeding the aneurysm. A similar flow characteristic was observed in a patient-specific basilar artery aneurysm by Mut et al. [Mut, Löhner, Chien et al. (2011)], who found the main impingement region at the centre of the aneurysmal neck accompanied by low WSS at the aneurysmal dome due to the direction of the basilar artery aneurysm matching the direction of blood flow in the basilar artery.

With the disappearance of the aneurysmal sac after clipping, the blood flow was markedly changed. The vortex inside the aneurysm disappeared and a new impingement site arose mainly at the wall of the ACoA. We can see that local high pressure in the aneurysm branch is at the new impingement region close to the clipping location in all three cases. After clipping there is lower WSS in the new impingement region and higher WSS surrounding its new impingement.

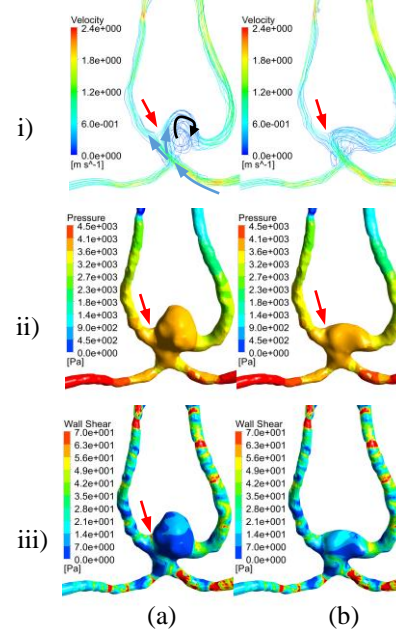


**Figure 8:** (Case 1): (i) Streamline, (ii) Velocity and (iii) WSS distribution of an ACoA aneurysm with an aneurysm angle of  $\theta=15^\circ$  (a) before and (b) after virtual clipping

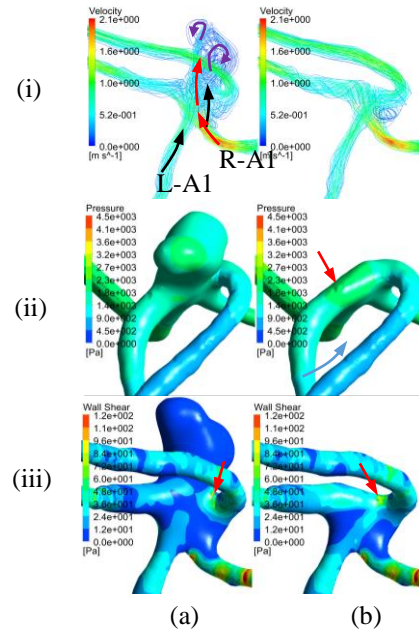


**Figure 9:** (Case 2): (i) Streamline, (ii) Pressure and (iii) WSS distribution of an ACoA aneurysm with an aneurysm angle of  $\theta=80^\circ$  (a) before and (b) after virtual clipping

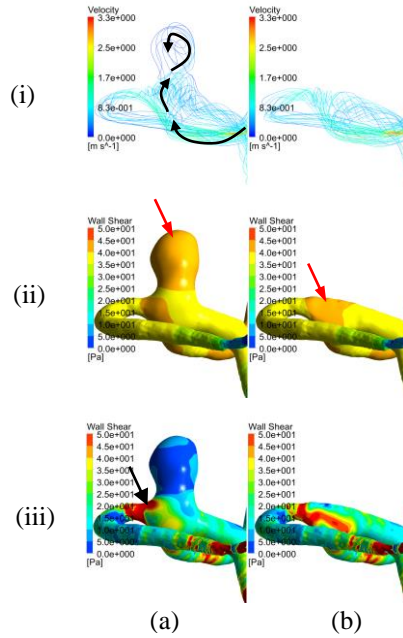


**Figure 10:** (Case 3): (i) Streamline, (ii) Pressure and (iii) WSS distribution of an ACoA aneurysm with an aneurysm angle of  $\theta=120^\circ$  (a) before and (b) after virtual clipping

### 3.2 Flow dynamics analysis in the aneurysms with different clipping location based on two clipping strategies

As demonstrated by Wang et al. [Wang, Xu and Xu (2017)] and Nossek et al. [Nossek, Setton, Karimi et al. (2016)], clipping an aneurysm with a small aneurysmal angle is challenging. In particular, for reconstructing an ACoA aneurysm with a neck wider than 3 mm, two clips are often set parallel to ACoA in opposite direction. The effect of aneurysm treatment will be influenced by the relative positions of these two clips, as shown in Section 3.2.1. For the treatment of an aneurysm with large aneurysmal angle, a straight clip is usually set parallel to ACoA, which does not locate in the virtual two-dimensional plane, as shown in Section 3.2.2 and Section 3.2.3. The maximum of WSS and pressure in the five samples with different aneurysmal angles were obtained to discuss a primarily statistical result about the effect of clipping angle on hemodynamic factors of ACoA whose aneurysmal angle ranges from  $70^\circ$  to  $120^\circ$ , as shown in Section 3.2.4

#### 3.2.1 Case 1: Aneurysm angle $\theta=15^\circ$ with different clipping locations

Fig. 11a presents the ACoA aneurysm model after clipping at these three different locations. Angle  $\beta$  represents the directions of clips. We noticed that a residual portion of the aneurysm neck is generated by non-parallel clips. It was found that as the angle of the clips decreased, the residual neck of the aneurysm increased. Figs. 11b and 11c compare the WSS, streamline and pressure distributions in the aneurysm with different clip locations ( $\beta=170^\circ$ ,  $160^\circ$  and  $145^\circ$ ). While there is no obvious change in local maximum pressure ( $3.357 \times 10^3$  Pa,  $3.360 \times 10^3$  Pa and  $3.365 \times 10^3$  Pa, respectively), the region of high

pressure becomes smaller as the residual neck of the aneurysm is reduced. The maximum WSS at the aneurysmal neck in the three cases is 65.0 Pa, 75.8 Pa and 65.9 Pa, respectively, much lower than the maximum WSS of 84.0 Pa without clipping. For the two clips set closer to the horizontal line ( $\beta=170^\circ$ ), the WSS distribution is more uniform than that in other cases. The maximum WSS value was obtained by calculating the WSS at the maximum node and the eight surrounding nodes using the FLUENT probing function [Chi, He, Luan et al. (2017)].

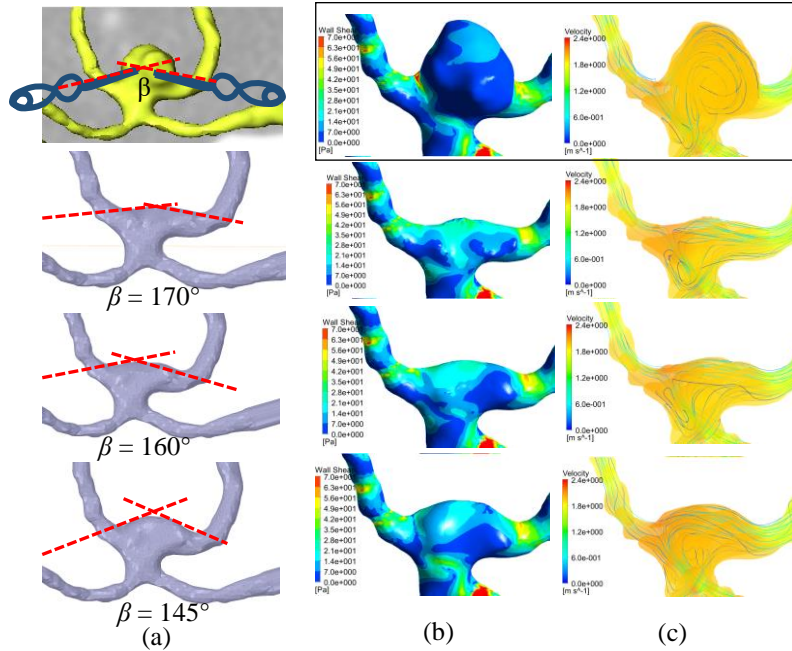


**Figure 11:** Case 1: Comparison of flow characteristics before and after clipping surgery using two clips for an aneurysm angle of  $\theta=15^\circ$  at different clipping angles  $\beta$ : (a) Location of clipping and 3D model of the ACoA aneurysm after clipping, (b) WSS distribution, and (c) Streamline and pressure indicated by color

### 3.2.2 Case 2: Aneurysm angle $\theta=80^\circ$ with different clipping locations

For the case of ACoA aneurysm with an aneurysm angle of  $\theta=80^\circ$ , the aneurysm is considered to be supplied by both left A1 segment (L-A1) and right A1 segment (R-A1) according to the streamline distribution in Fig. 9. Moreover, we considered L-A1 is the main dominance of A1 segment of ACA. A reason is that the aneurysmal direction is almost coincidence with the flow direction of L-A1. And the inflow region of aneurysm from L-A1 is closer to the middle of aneurysm than that from R-A1, as the red and black arrow shows in Fig. 9. Another reason is that the diameter of L-A1 is larger than that in R-A1. It has been reported that the vascular diameter in the dominance of A1 segment of ACA is larger than the size of another A1 segment in anatomy. Three clipping planes for treating this aneurysm were then adopt as follow: a) Normal to the flow direction in the proximal L-A1; b) Normal to aneurysmal direction; and c) An angle of clipping direction

$\alpha=20^\circ$  to aneurysmal direction.  $\alpha$  was defined by the normal line of clipping plane to the aneurysmal direction, as shown in the inset of Fig. 12.

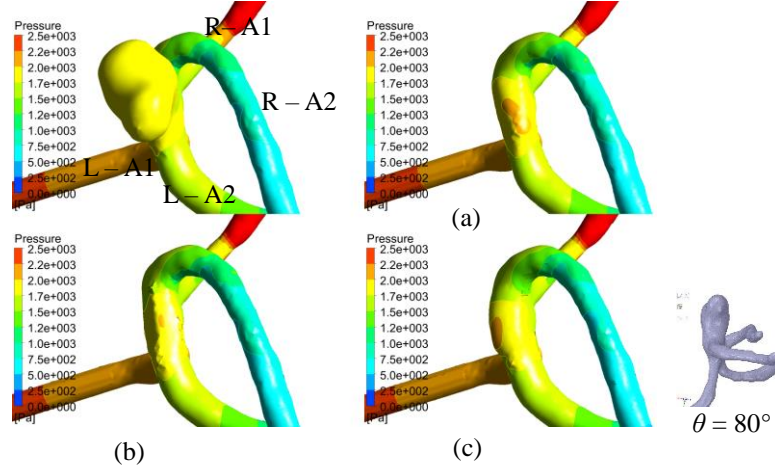


**Figure 12:** Case 2: Pressure distribution in the aneurysm for ( $\theta=80^\circ$ ) before and after clipping. The clipping plane is (a) Normal to the flow direction in L-A1, (b) Normal to aneurysmal direction, and (c) An angle of  $\alpha=20^\circ$  to the aneurysmal direction

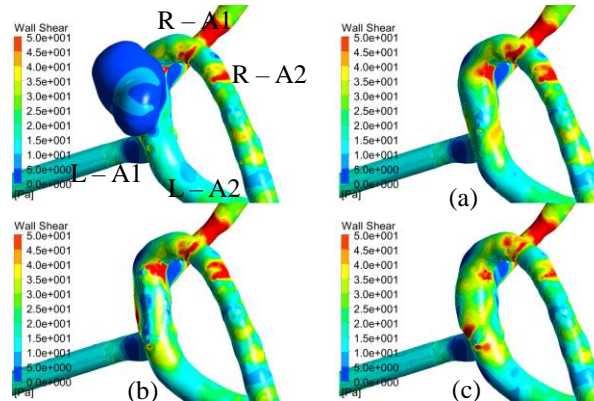


**Figure 13:** Case 2: WSS distribution in the aneurysm for ( $\theta=80^\circ$ ) before and after clipping. The clipping plane is (a) Normal to the flow direction in L-A1, (b) Normal to aneurysmal direction, and (c) An angle of  $\alpha=20^\circ$  with the aneurysmal direction

The structure of the aneurysm vessel is modified by the clip [Wang, Xu and Xu (2017)], which affects the subsequent pressure and WSS distribution of the aneurysm. Fig. 12 shows the comparison of pressure distribution in the aneurysm after clipping surgery with different clipping locations. We noticed that the local high pressure raises at the aneurysmal wall with clip. When the clipping plane is normal to the inflow direction of aneurysm, the area of local high pressure is the largest in all three clip locations as the dotted line indicated. In addition, by comparing the WSS distribution of aneurysm after clip in Fig. 13, we found that there are increases of WSS at the aneurysm region. Merely,

there are no clear differences of WSS among the three clipping locations. Around the clipping locations, the maximum of WSS is (a) 74.59 Pa, (b) 77.92 Pa and (c) 69.75 Pa, and the minimum of WSS is (a) 5.41 Pa, (b) 5.73 Pa and (c) 6.70 Pa respectively. We cannot give a judgement on which clipping location is better than others if WSS distribution was only considered. We may suggest that there could be a negative effect on the clipping fastness due to much wider region of high pressure at the clipping location when the clipping plane is normal to the flow direction of dominance of A1 segment (Location (a)).

### 3.2.3 Case 3: Aneurysm angle $\theta=120^\circ$ with different clipping locations

For the aneurysm angle of  $\theta=120^\circ$ , three different directions of clipping the aneurysm were considered as follow: a) Along the inflow direction of aneurysm from the A1 segment; b) The same direction of the aneurysmal dome; and c) An angle  $\alpha=20^\circ$  of clipping direction to direction of aneurysmal dome, as shown in the inset of Fig. 14.

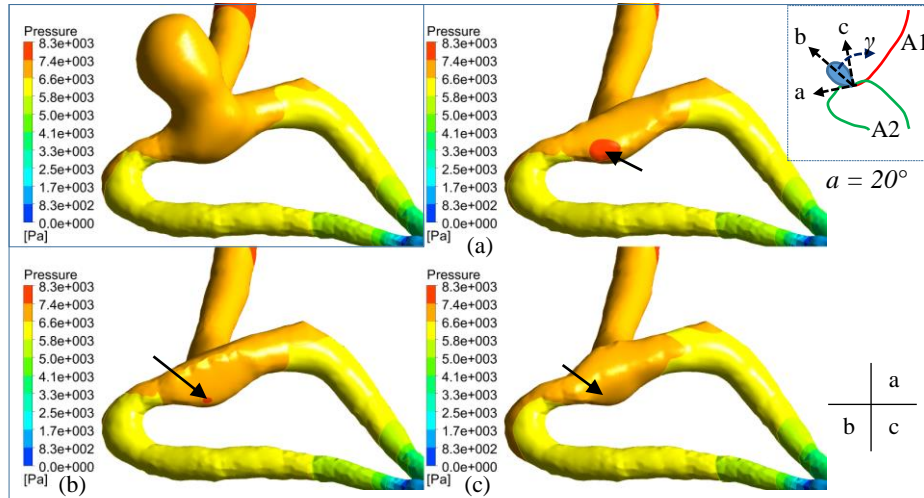


**Figure 14:** Case 3: Pressure distribution in the aneurysm for ( $\theta=120^\circ$ ) without and with clipping treatment. The clipping direction follows (a) The flow direction in the A1 segment, (b) The direction of the aneurysmal dome, and (c) The direction of b with a rotation of an angle  $\alpha=20^\circ$

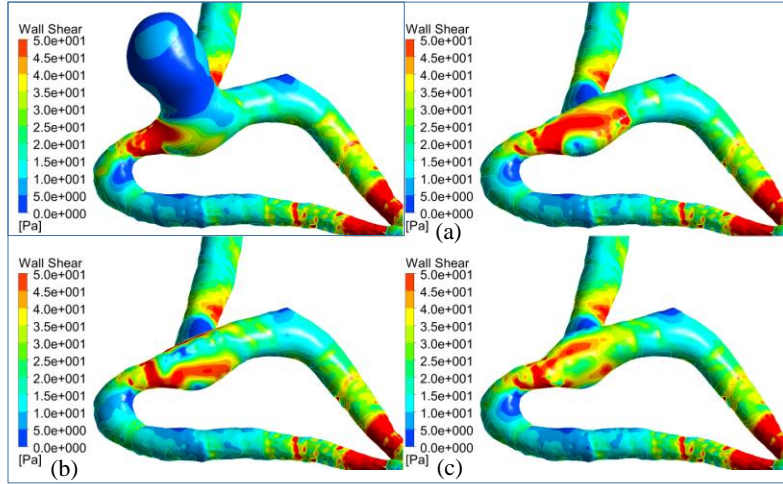


**Figure 15:** Case 3: WSS distribution in the aneurysm before and after clipping. The clipping direction follows (a) The flow direction of the A1 segment, (b) The direction of the aneurysmal dome, (c) The direction of b with a rotation of an angle  $\alpha=20^\circ$

Figs. 14 and 15 show comparisons of pressure and WSS distribution in the aneurysm without and with clipping surgery at the different clipping locations. The maximum pressure value in the three cases is  $7.55 \times 10^3$  Pa,  $7.45 \times 10^3$  Pa, and  $7.30 \times 10^3$  Pa, respectively. The high pressure still rises at the new impingement region after clipping, it is worth noting that the maximum pressure changes with the clipping location. When the clipping direction follows the inflow direction of aneurysm from the A1 segment (a), the maximum pressure is about 1.2 times higher than in other clipping ways. In addition, comparing the WSS distribution around the clipping region in the ACoA aneurysm with three clipping location, the maximum of WSS is (a) 73.30 Pa, (b) 53.28 Pa, and (c) 53.08 Pa respectively. The area with high WSS around the new impingement region is largest comparing that in other clipping locations when the clipping direction follows the flow direction of the proximal A1 segment (Location (a)).

### 3.2.4 Hemodynamic differences on the aneurysms with different clip angles

Fig. 16 shows the maximum of WSS and pressure with the three clipping aneurysmal angles in five samples, which are nondimensionalized by the maximum of WSS ( $WSS_{max\_a}$ ) and pressure ( $p_{max\_a}$ ) around the clip normal to the flow direction in A1 (Clip a) in each sample. It can be found that, for the clip normal to inflow direction of aneurysm supplied by A1, the maximum of WSS is not always larger than that in other two clipping situations. WSS distribution would depend on the geometry of aneurysm after clipping treatment. When the clip plane is normal to the blood flow direction in A1, the maximum of pressure is largest comparing to other two clipping ways in four out of five samples due to its impingement of flow close to clip location. It means that a good clipping location would be chosen to avoid the impingement of inflow from A1 segment.

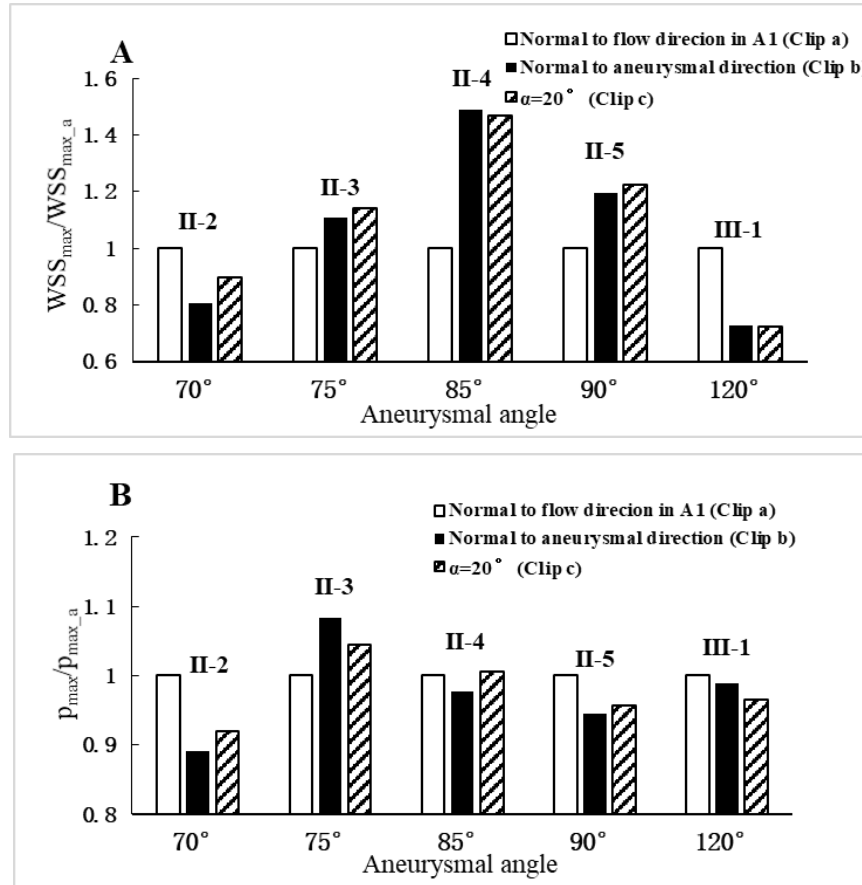


**Figure 16:** A) WSS maximum and B) pressure maximum around the clip location for different clipping angles, nondimensionalized by the maximum of WSS ( $WSS_{max\_a}$ ) and pressure ( $p_{max\_a}$ ) around the clip normal to the flow direction in A1 (Clip a) in each sample

## 4 Discussion and limitations

### 4.1 Discussion

Surgical clipping is one of the most common methods for treating intracranial aneurysm, and the decision of a surgical strategy is frequently dependent on the topology of ACoA aneurysmal structure. For clipping the aneurysm with a small aneurysmal angle with a wide neck, two or more clips were often aligned in opposite ways paralleled to ACoA to reshape the aneurysm neck [Nossek, Setton, Karimi et al. (2016); Wang, Xu and Xu (2017)]. As the Case 1 analyzed in this study, with the clipping angle close to the angle of 180°, the treatment would be better with more uniform WSS distribution than that in the aneurysms with other angles of clips. And for clipping the aneurysm whose dome projected away from the plane created by the A2 segments without rotation of this plane, such as the ACoA aneurysms in the Case 2 and Case 3, the clip was usually placed at the aneurysm neck parallel to the ACoA [Nossek, Setton, Karimi et al. (2016); Wang, Xu and

Xu (2017)].

In addition, aneurysmal morphological characteristic included aneurysm site, dominance of A1 segment of ACA, and direction of aneurysm dome around the ACoA were mainly considered in clinic [Hernesniemi, Dashti, Lehecka et al. (2008b); Nossek, Setton, Karimi et al. (2016); Wang, Xu and Xu (2017)]. The selections of clip type and clipping location always required experiences of doctors in microneurosurgical clipping of ACoA aneurysms [Hernesniemi, Dashti, Lehecka et al. (2008b)]. We observed that clipping locations clearly influenced the local WSS and pressure distribution from the situation. When the clipping direction followed the bending direction of the dominance of A1 segment, a new high-pressure impingement region will appear at the clipping location with high WSS around it. And when the clipping plane is normal to the flow direction of A1, wide WSS region and high pressure distribution are more likely to appearance at the implementation region close to the clip.

Furthermore, it was reported that the loose clip or clip slipping after microneurosurgery in clinic will cause the aneurysm recanalized [Wu, Yang, Huang et al. (2013b)], however, there were few researches on the hemodynamic simulation of aneurysm with clipping treatment. Several studies have reported that high-flow velocity and WSS might be associated with the recanalization of aneurysm after embolization. They found that the high-velocity and WSS region exactly corresponded with the location of aneurysm recanalization. Chen et al. [Chen, Wang, Ding et al. (2009)] pointed out that the maximum WSS appeared in the middle of aneurysm wall at the systolic peak after the aneurysm treatment with embolization. Ortega et al. [Ortega, Hartman, Rodriguez et al. (2008)] found the increase in WSS under the portion of embolization. Irie et al. [Irie, Anzai, Kojima et al. (2012)] found that there was higher pressure at the enlarged aneurysm wall than that at the neck after embolization of aneurysm. They considered that high pressure caused by high-flow velocity may lead to coil compaction which was one of the reasons for the aneurysm recanalization. We may also speculate that high pressure at the clipping location would be harmful for the fastness of clip under the long-term impact of high-speed blood flow. It is therefore suggested that a good surgical option would be to locate the clip away from the flow direction of the main A1 segment supplying the aneurysm. On the other hand, due to limited operating space and the complexity of blood vessel structure, there are few choices for the clipping locations under clinical conditions. In any cases, we should choose the clipping location to avoid the impingement of inflow from A1 segment as possible as we can.

#### **4.2 Limitations**

In the patient-specific study, we made several simplifications and assumptions. The first relates to the simplified computational model of the aneurysmal branch without considering the full circle of Willis. Flow distribution will be affected by the contralateral regulation of cerebral blood flow in a fully functional circle of Willis. In addition, we considered the blood vessel as a rigid wall, thus neglecting the interaction between the flow and wall structure. Further, the steady-state simulation can reveal the behavior of high WSS in the models, unsteady-state simulations are preferable when computational cost is not a consideration [Chi, He, Luan et al. (2017)]. Moreover, the aneurysmal

structure after virtual surgical clipping should be verified by comparing with the reconstruction of aneurysmal structure based on the original CT imaging data of patient after aneurysmal clipping. And we will collect more ACoA aneurysms to discuss the anatomical structure effects on the hemodynamic factors and gain statistical results using all geometries in the future work.

## 5 Conclusions

In this study, we have simulated the hemodynamic properties of three patient-specific ACoA aneurysms with different aneurysmal angles before and after the clipping treatment with three clipping locations.

The results show that high pressure rises at impingement region of an ACoA aneurysm in clipping treatment, accompanying with high WSS around this region, and the impingement region depends on clipping locations. Moreover, the highest pressure with non-uniform WSS distribution appears at the impingement region close to the clipping location when the clipping direction follows the direction of the flow in A1 segment which supplies the aneurysm mainly. It had better to avoid the impingement region during the clipping treatment for choosing the clipping locations.

To obtain more information about the effect of clipping location on flow characteristics in the micosurgical treatment, we will analyze more patient-specific aneurysmal cases with more different clipping locations in the future work. It would preoperatively give a useful information to the decision of surgical plan.

**Acknowledgement:** This work was kindly supported by National Natural Science Foundation of China (11602053, 51576033), and Education Department of Liaoning Province general project (L2015113).

## References

- Ahmed, S.; Šutalo, I. D.; Kavnoudias, H.** (2006): Hemodynamics and stress distribution in a cerebral aneurysm partially blocked with coils. *Fifth International Conference on CFD in the Process Industries*.
- Alastruey, J.; Parker, K. H.; Peiró, J.; Byrd, S. M.; Sherwin, S. J.** (2007): Modelling the circle of Willis to assess the effects of anatomical variations and occlusions on cerebral flows. *Journal of Biomechanics*, vol. 40, no. 8, pp. 1794-1805.
- Amp, P. P. C. M.; Dobos, P.** (2014): An *in vitro* assessment of the cerebral hemodynamics through three patient specific circle of Willis geometries. *Journal of Biomechanical Engineering*, vol. 136, no. 1.
- Arcaute, K.; Wicker, R. B.** (2008): Patient-specific compliant vessel manufacturing ssing dip-spin coating of rapid prototyped molds. *Journal of Manufacturing Science & Engineering*, vol. 130, no. 5, pp. 1-13.
- Byun, H. S.; Rhee, K.** (2004): CFD modeling of blood flow following coil embolization of aneurysms. *Medical Engineering & Physics*, vol. 26, no. 9, pp. 755-761.
- Campi, A.; Ramzi, N.; Molyneux, A. J.; Summers, P. E.; Kerr, R. S. C. et al.** (2007): Retreatment of ruptured cerebral aneurysms in patients randomized by coiling or clipping in

- the international subarachnoid aneurysm trial (ISAT). *Stroke*, vol. 38, no. 5, pp. 1538-1544.
- Chen, J.; Wang, S.; Ding, G.; Yang, X.; Li, H.** (2009): Patient-specific blood dynamic simulations in assessing endovascular occlusion of intracranial aneurysms. *Journal of Hydrodynamics, Series B*, vol. 21, no. 2, pp. 271-276.
- Chen, J.; Wang, S.; Ding, G.; Yang, X.; Li, H.** (2009): The effect of aneurismal-wall mechanical properties on patient-specific hemodynamic simulations: Two clinical case reports. *Acta Mechanica Sinica*, vol. 25, no. 5, pp. 677-688.
- Cheng, Z.; Tan, F. P.; Riga, C. V.; Bicknell, C. D.; Hamady, M. S. et al.** (2010): Analysis of flow patterns in a patient-specific aortic dissection model. *Journal of Biomechanical Engineering*, vol. 132, no. 5.
- Chi, Q.; He, Y.; Luan, Y.; Qin, K.; Mu, L.** (2017): Numerical analysis of wall shear stress in ascending aorta before tearing in type an aortic dissection. *Computers in Biology & Medicine*, vol. 236, no. 89, pp. 236-247.
- Chodzyński, K. J.; Eker, O. F.; Vanrossomme, A. E.; de Sousa, D. R.; Coussément, G. et al.** (2016): Does the gravity orientation of saccular aneurysms influence hemodynamics? An experimental study with and without flow diverter stent. *Journal of Biomechanics*, vol. 49, no. 16, pp. 3808-3814.
- Cieslicki, K.; Ciesla, D.** (2005): Investigations of flow and pressure distributions in physical model of the circle of Willis. *Journal of Biomechanics*, vol. 38, no. 11, pp. 2302-2310.
- Geers, A. J.; Larrabide, I.; Morales, H. G.; Frangi, A. F.** (2014): Approximating hemodynamics of cerebral aneurysms with steady flow simulations. *Journal of Biomechanics*, vol. 47, no. 1, pp. 178-185.
- Gobin, Y. P.; Counord, J. L.; Flaud, P.; Duffaux, J.** (1994): *In vitro* study of haemodynamics in a giant saccular aneurysm model: Influence of flow dynamics in the parent vessel and effects of coil embolisation. *Neuroradiology*, vol. 36, no. 7, pp. 530-536.
- Hernesniemi, J.; Dashti, R.; Lehecka, M.; Niemelä, M.; Rinne, J. et al.** (2008a): Microneurosurgical management of anterior communicating artery aneurysms. *Surgical Neurology*, vol. 70, no. 1, pp. 8-28.
- Irie, K.; Anzai, H.; Kojima, M.; Honjo, N.; Ohta, M. et al.** (2012): Computational fluid dynamic analysis following recurrence of cerebral aneurysm after coil embolization. *Asian Journal of Neurosurgery*, vol. 7, no. 3, pp. 109-115.
- Jhunjhunwala, P.; Padole, P. M.; Thombre, S. B.** (2016): Non-Newtonian blood flow in left coronary arteries with varying stenosis: A comparative study. *Molecular & Cellular Biomechanics*, vol. 1313, no. 11, pp. 1-261.
- Jou, L.; Lee, D. H.; Mawad, M. E.** (2010): Cross-flow at the anterior communicating artery and its implication in cerebral aneurysm formation. *Journal of Biomechanics*, vol. 43, no. 11, pp. 2189-2195.
- Karmonik, C.; Diaz, O.; Klucznik, R.; Grossman, G. R.; Zhang, J. Y. et al.** (2014): Quantitative comparison of hemodynamic parameters from steady and transient CFD simulations in cerebral aneurysms with focus on the aneurysm ostium. *Journal of NeuroInterventional Surgery*, vol. 7, no. 5, pp. 367-372.
- Khan, M. O.; Valen-Sendstad, K.; Steinman, D. A.** (2015): Narrowing the expertise

gap for predicting intracranial aneurysm hemodynamics: Impact of solver numerics versus mesh and time-step resolution. *American Journal of Neuroradiology*, vol. 36, no. 7, pp. 1310-1306.

**Kim, B. M.; Shin, Y. S.; Kim, S. H.; Suh, S. H.; Ihn, Y. K. et al.** (2011): Incidence and risk factors of recurrence after endovascular treatment of intracranial vertebrobasilar dissecting aneurysms. *Stroke*, vol. 42, no. 9, pp. 2425-2430.

**Kousera, C. A.; Wood, N. B.; Seed, W. A.; Torii, R.; O'Regan, D. et al.** (2013): A numerical study of aortic flow stability and comparison with *in vivo* flow measurements. *Journal of Biomechanical Engineering*, vol. 135, no. 1.

**Lasheras, J. C.** (2007): The biomechanics of arterial aneurysms. *Annual Review Fluid Mechanics*, vol. 39, pp. 293-319.

**Liu, Z.; Cai, Y.; Chen, G. Z.; Lu, G. M.; Li, Z. M.** (2017): Anatomical variations in circle of Willis and intracranial aneurysm formation. *Molecular & Cellular Biomechanics*, vol. 14, no. 1, pp. 19-31.

**Luo, B.; Yang, X.; Wang, S.; Li, H.; Chen, J. et al.** (2011): High shear stress and flow velocity in partially occluded aneurysms prone to recanalization. *Stroke*, vol. 42, no. 3, pp. 745-753.

**Mantha, A. R.; Benndorf, G.; Hernandez, A.; Metcalfe, R. W.** (2009): Stability of pulsatile blood flow at the ostium of cerebral aneurysms. *Journal of Biomechanics*, vol. 42, no. 8, pp. 1081-1087.

**Mashiko, T.; Otani, K.; Kawano, R.; Konno, T.; Kaneko, N. et al.** (2015): Development of three-dimensional hollow elastic model for cerebral aneurysm clipping simulation enabling rapid and low cost prototyping. *World Neurosurgery*, vol. 83, no. 3, pp. 351-361.

**Matsukawa, H.; Uemura, A.; Fujii, M.; Kamo, M.; Takahashi, O. et al.** (2013): Morphological and clinical risk factors for the rupture of anterior communicating artery aneurysms. *Journal of Neurosurgery*, vol. 118, no. 5, pp. 978-983.

**Molyneux, A.; Kerr, R.; Stratton, I.; Sandercock, P.; Clarke, M. et al.** (2002): International Subarachnoid Aneurysm Trial (ISAT) of neurosurgical clipping versus endovascular coiling in 2143 patients with ruptured intracranial aneurysms: a randomised trial. *Journal of Stroke and Cerebrovascular Diseases*, vol. 11, no. 6, pp. 304-314.

**Mut, F.; Löhner, R.; Chien, A.; Tateshima, S.; Viñuela, F. et al.** (2011): Computational hemodynamics framework for the analysis of cerebral aneurysms. *International Journal for Numerical Methods in Biomedical Engineering*, vol. 27, no. 6, pp. 822-839.

**Nossek, E.; Setton, A.; Karimi, R.; Dehdashti, A. R.; Langer, D. J. et al.** (2016): Analysis of superiorly projecting anterior communicating artery aneurysms: Anatomy, techniques, and outcome. A proposed classification system. *Neurosurgical Review*, vol. 39, no. 2, pp. 225-235.

**Olivieri, L. J.; Zélicourt, D. A. D.; Haggerty, C. M.; Ratnayaka, K; Cross, R. R. et al.** (2011): Hemodynamic modeling of surgically repaired coarctation of the aorta. *Cardiovascular Engineering & Technology*, vol. 2, no. 4, pp. 288-295.

- Ortega, J.; Hartman, J.; Rodriguez, J.; Maitland, D.** (2008): Post-treatment hemodynamics of a basilar aneurysm and bifurcation. *Annals of Biomedical Engineering*, vol. 36, no. 9, pp. 1531-1546.
- Lai, S. S.; Tang, A. Y.; Tsang, A. C.; Leung, G. K.; Yu, A. C. et al.** (2016): A joint computational-experimental study of intracranial aneurysms: Importance of the aspect ratio. *Journal of Hydrodynamics*, vol. 28, no. 3, pp. 462-472.
- Teleb, M. S.; Pandya, D. J.; Castonguay, A. C.; Eckardt, G.; Sweis, R. et al.** (2014): Safety and predictors of aneurysm retreatment for remnant intracranial aneurysm after initial endovascular embolization. *Journal of Neurointerventional Surgery*, vol. 6, no. 7, pp. 490-494.
- Ujiie, H.; Tachibana, H.; Hiramatsu, O.; Hazel, A. L.; Matsumoto, T. et al.** (1999): Effects of size and shape (aspect ratio) on the hemodynamics of saccular aneurysms: a possible index for surgical treatment of intracranial aneurysms. *Neurosurgery*, vol. 45, no. 1, pp. 119-129.
- Ujiie, H.; Tamano, Y.; Sasaki, K.; Hori, T.** (2001): Is the aspect ratio a reliable index for predicting the rupture of a saccular aneurysm? *Neurosurgery*, vol. 48, no. 3, pp. 495-502.
- Wang, J.; Xu, F.; Xu, B.** (2017): Classification and clipping strategy of superior projecting anterior communicating artery aneurysms. *Journal of Clinical Neurosurgery*, vol. 14, no. 3, pp. 163-167.
- Wu, Q. J.; Yang, P. F.; Huang, Q. H.; Liu, J. M.** (2013a): Risk factor analysis and progress on treatment of recurrent cerebral aneurysms after endovascular treatment. *Chinese Journal of Stroke*, vol. 8, no. 11, pp. 899-903.
- Xu, L.; Zhang, F.; Wang, H.; Yu, Y.** (2012): Contribution of the hemodynamics of A1 dysplasia or hypoplasia to anterior communicating artery aneurysms: A 3-dimensional numerical simulation study. *Journal of Computer Assisted Tomography*, vol. 36, no. 4, pp. 421-426.